scientific reports

OPEN

Deterministic field-free voltage-induced magnetization switching with self-regulated precession for low-power memory

Stanislav Sin & Saeroonter Oh✉

Spintronic devices are regarded as a promising solution for future computing and memory technologies. They are non-volatile, resilient to radiation, and compatible with the CMOS back-end process. However, the major drawbacks of modern current-driven spintronic devices are the long switching delay and relatively high power consumption. Recent progress in magnetoelectronics, particularly in voltage-controlled magnetism reveals a possible solution. Voltage-controlled magnetic anisotropy (VCMA) allows the manipulation of interface-mediated perpendicular anisotropy energy. However, most VCMA-based switching methods require pre-read operation, precise pulse-width control and have high write error rate. This study proposes a novel deterministic self-regulated precessional ferromagnet switching method, which overcomes these issues. In the discussed method, energy symmetry is broken by a dependence of MTJ resistance on the angle between magnetization vectors of free and pinned layers. Hence, the method does not require an external magnetic field and large electric current. The proposed method is verified through micromagnetic simulations and benchmarked with other methods typically reported in the literature. We report the write error rate is significantly improved compared to other VCMA switching methods. Moreover, the mean energy consumption is as low as 38.22 fJ and the mean switching delay is 3.77 ns.

Density of 2D scaling of conventional transistors and memory devices are either slowing or expanding into the third dimension. Hence, a large number of studies is devoted to technologies which will augment current silicon devices or will be used in emerging computing architectures, such as monolithic integration of logic and memory, compute-in-memory, neuromorphic computing, and probabilistic computing. One of these promising technologies is spintronics[1–7]. Spintronic devices are non-volatile, resilient to radiation, and most importantly, they are compatible with the CMOS back-end process. Spintronic memory can be used as a non-volatile alternative to low-level cache, embedded memory, or a new class of memory[5]. However, there are several challenges to a broad application of spintronics in modern computing, such as long switching delay and large power consumption due to their current-driven operation.

Recently-discovered voltage-controlled magnetic anisotropy (VCMA) effect may become a viable solution to these challenges. Voltage-induced charge at the magnet/oxide interface reduces magnetic anisotropy energy, allowing a lower barrier for magnetization switching[2–5,8–11]. However, VCMA alone cannot perform a 180° switching, and it is used as an assistance to other symmetry breaking-mechanisms. Such a mechanism can be an external magnetic field (ExMF) combined with time-domain asymmetry, spin-transfer torque (STT), or spin-orbit torque (SOT).

Symmetry-breaking by means of ExMF results in a magnetic field-assisted precessional voltage-induced (MFPV) switching method[4,8–14]. In this switching, a short voltage pulse lowers the energy barrier, whereas the ExMF creates energy minima in the plane direction, thus generating a precession. If the pulse timing is right, the precession should finish when magnetization reaches the opposite state. This method results in a sub-nanosecond and low-power magnetization switching, which is attractive. But it also has several drawbacks such as precise pulse timing requirement, non-deterministic bit writing (MTJ can only toggle its state and requires a pre-read operation), and high write error rate (WER)[14–16]. Moreover, current-generated ExMF introduces additional power consumption and leads to cross-talk between adjacent cells. Hence, many efforts are devoted to realize a field-free magnetization switching. Recent studies show that the addition of an antiferromagnetic layer on top

Department of Electrical and Electronic Engineering, Hanyang University, Ansan 15588, Korea. ✉email: sroonter@hanyang.ac.kr

of the MTJ can induce an effective in-plane field with a magnitude of ~4000 A/m[17–19]. Additionally, the in-plane term of demagnetizing energy can assist the precession[13,20,21]. Both effects can be used for a field-free precessional voltage-induced (FFPV) switching method. Note that in this work, the term "field-free" implies an absence of ExMF. FFPV eliminates the need for a conducting wire, thus improving cell scalability and simplifying the device design; however, other issues of MFPV remain unsolved. Hence, complex error correction circuitry with self-adjustment and self-termination should be used for precessional switching[22–25].

It is also possible to divide a voltage pulse into two sub-pulses: the first sub-pulse having enough magnitude to start a precession, whereas a lower second pulse is used to inject a small amount of STT. This method is referred to as precessional STT-assisted (PSTT) switching[4,12,14,26]. PSTT is a field-free and relatively fast switching; however, since it relies on STT, its power efficiency is slightly worse compared to the purely precessional methods. Improper sub-pulse timings theoretically may lead to a false switching, but the timing requirement is not as strict as for MFPV and FFPV.

In-plane field from antiferromagnet can be used for SOT switching of MTJs with perpendicular magnetization[17–19,27–29]. Moreover, external voltage can be applied across the MTJ to utilize barrier lowering from the VCMA effect. This method is referred to as voltage-assisted SOT (VSOT) switching. The advantage of the VSOT method is that it has a separated low-resistivity path for SOT current and a high-resistivity path for voltage. Consequently, pulses used for SOT and VCMA can be injected simultaneously. It allows deterministic, sub-nanosecond switching, but the current density in SOT material is typically on the order of MA/cm^2.

Recently, Wu et al. proposed a deterministic and field-free, voltage-induced (DFFV) ferromagnet switching[30]. In their work, energy symmetry was broken by the perpendicular stray field from the synthetic antiferromagnet stack. The magnet is switched from the parallel (P) to the antiparallel (AP) state using a single-pulse voltage, but for AP→P switching a double-pulse voltage is required. Experimental measurements demonstrated sub-nanosecond delay with 20 fJ energy consumption. However, due to the uncompensated stray field, thermal stability factor Δ decreases with respect to the nominal value. Hence, a relatively low WER of $\sim 10^{-4}$ was shown.

In this study, an alternative deterministic field-free switching method is proposed, which utilizes the the fact that $R_{ap} > R_p$ for breaking the energy symmetry. The proposed deterministic field-free self-regulated precessional (DFFSP) method utilizes a double-barrier MTJ configuration, which has high thermal stability and high TMR[31]. Micromagnetic simulations were performed to verify the device operation. We found that the switching delay does not monotonically decrease with current but exhibits oscillating behavior due to the formation of local energy minima along the x-axis, revealed by magnetic energy contour maps. Finally, the performance of DFFSP was benchmarked using Monte Carlo simulations and compared with those of other methods.

Results

Proposed deterministic field-free magnetization switching with self-regulated precession

Figure 1a shows the double-barrier MTJ structure for the proposed DFFSP switching scheme. The free layer (FL) is sandwiched between two pinned layers (PLs), which are separated from each other by a tunneling barrier. PL1 (PL in MTJ1) and PL2 (PL in MTJ2) are magnetized in $+z$ and $-z$ direction, respectively. The device has three terminals: FL is connected to the ground (through terminal T3), whereas PL1 and PL2 are connected to the top (T1) and bottom (T2) terminals, respectively. We assume a generic double-barrier MTJ stack[31–36]: Ta/{[Co/Pt]/Co/Ru/Co/[Co/Pt]} (SAF layer)/Co/Ta/CoFeB (PL1)/MgO/[CoFeB/W/CoFeB] (FL)/MgO/CoFeB (PL2)/Ta/{Co/[Co/Pt] /Co/Ru/Co[Co/Pt]} (SAF layer)/Ta. The double MTJ structure takes advantage of having two oxide/FL interfaces, hence the doubled effective interface anisotropy, compared to the conventional MTJ. A composite CoFeB/W/CoFeb FL layer is used since a thin W spacer further improves interfacial anisotropy of the layer.

The fabrication of such a stack may be difficult since it requires attaching a contact to the FL deposited between PL1 and PL2. We suggest to slightly extend FL out of the main stack. The excessive length of FL can be used for contact formation. In this study we analyze the theoretical upper limit of the DFFSP, thus we assume the extension length of FL is so small that it has almost no effect on the device performance.

As shown in Fig. 1b, writing the "up" state and read operations are performed by feeding a constant current through MTJ1 (connected between T1 and T3). The bias voltage across MTJ1 V_b will induce charge at the top oxide interface, which due to the VCMA effect will decrease perpendicular anisotropy by the amount $E_{VCMA} \propto I_{wup}R(\theta, V_b)/t_{ox}$, where I_{wup} denotes the current for writing the "up" state, t_{ox} denotes the oxide thickness, and R denotes the tunneling resistance which is the function of V_b and angle θ between the magnetization of PL1 and FL. The energy symmetry is broken due to the VCMA effect since the voltage $I_{wup} \cdot R_p < I_{wup} \cdot R_{ap}$, and if the current is large enough, magnetization will favor the P state. Similarly, MTJ2 allows deterministic writing of the "down" state, by injecting current through terminals T2 and T3 (see Fig. 1c). Figure 1d shows the energy plot for the MTJ1 at different currents. The magnetization reversal is possible for currents $I_{min} < I_{wup} < I_{max}$; however, energy minima is formed in $\pm x$-direction for $I_{wup} > I_{max}$ and switching becomes nondeterministic. Although electric current flows in the device, STT is not utilized. The sole purpose of current is to induce a charge in the oxide layer. Moreover, STT opposes precessional torque and is an unwanted effect in the proposed switching scheme.

Simulation results

To verify the DFFSP switching, micromagnetic simulations are performed. Table 1 shows FL parameters used in this study, which are based on experimental studies in the literature. As was mentioned before, double-barrier MTJ has almost two times larger interfacial anisotropy constant, which allows using a thicker FL. The advantage of thick FL is the higher in-plane term of demagnetizing field, which helps to switch the device faster.

Figure 2a–d show the magnetization dynamics under the influence of a current pulse with a duration of 50 ns. Here, the effect of random thermal field was excluded for clarity. Figure 2a shows that 3 μA current is insufficient

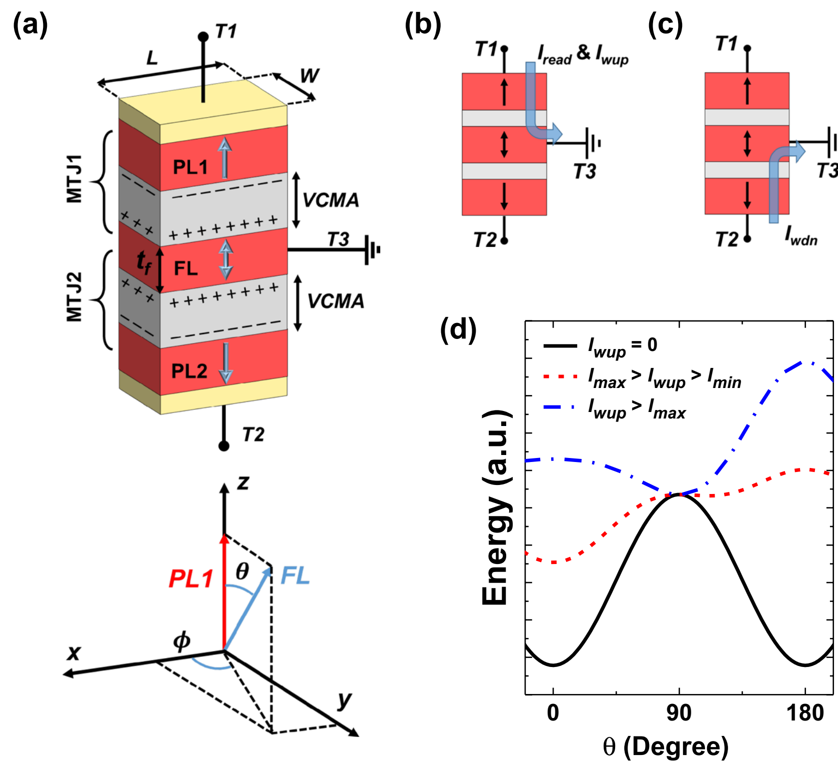

Figure 1. (**a**) Double-barrier MTJ stack for the DFFSP switching and reference coordinate system. (**b**) Writing the "up" state and read operations. The current is injected through terminals T1 and T3. (**c**) Writing the "down" state operation, current is injected through T2 and T3. (**d**) Energy plot for MTJ1 at different magnitudes of I_{wup}.

Symbol	Value	Description	Ref.
M_s	6.25×10^5 A/m	Saturation magnetization	[10]
Δ	60.0	Thermal stability factor	[10]
K_i	0.68 mJ/m^2 *	Interfacial anisotropy constant	[10]
ξ	100 fJ/V·m	VCMA coefficient	[37,38]
α	0.05	Damping constant	[4,16]
P	0.58	Spin polarization	[10]
$L \times W$	110×50 nm^2	Area of MTJ	
t_f	3.0 nm	Thickness of th FL	
t_{ox}	1.65 nm	Oxide thickness	
RA_p	758.7 $\Omega \cdot \mu$m^2	Resistance-area product	[39,40]
TMR	250%	Tunneling magnetoresistance	[39,40]
V_h	0.65 V	Voltage at which R_{ap} halves	[39,40]

Table 1. Simulation parameters for the free layer. *Note that interface anisotropy is doubled for a double-barrier MTJs[31–36].

for switching, therefore, such current can be used for the read operation. It induces voltage of 0.81 V and m_z establishes at -0.75. The current of 3.5 μA allows magnetization switching in approximately 4.6 ns. During the switching, voltage changes from 0.90 V in AP state to 0.48 V in P state. Magnetization switching also occurs at 4 μA, where voltage across the MTJ varies from 0.97 V to 0.55 V. However, magnetization oscillates back and forth before achieving the parallel state, which results in the switching delay to increase to $\approx$ 7 ns. The current of 5 μA induces 1.12 V. It leads to precession, and therefore, deterministic switching is not possible anymore. Such current dependence can be explained by means of energy contour maps.

The magnetization trajectories mapped on the energy contour plots in $\theta\phi$-plane are shown in Fig. 3a–d. As shown in Fig. 3a, at 3 μA a small energy barrier between AP and P states still exists and prevents switching. As shown in Fig. 3b, the barrier is eliminated at 3.5 μA, there is now an energy minimum at $\theta = 0°$, and switching is possible. It is also the case for 4 μA, but thanks to the demagnetizing energy, the local energy "pockets" are

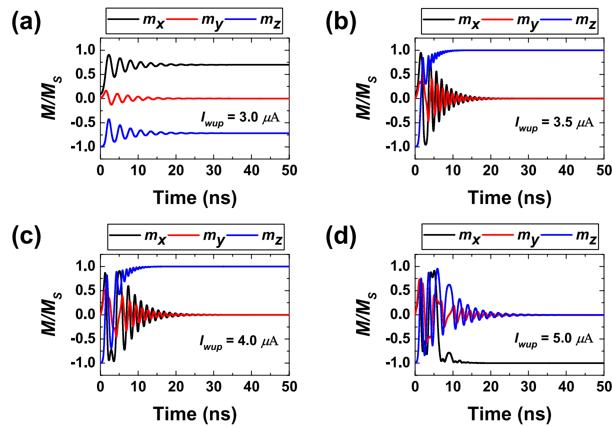

Figure 2. Temporal evolution of the normalized magnetization ($\boldsymbol{M}/M_s$) at I_{wup} of (**a**) 3 μA, (**b**) 3.5 μA, (**c**) 4 μA, and (**d**) 5 μA. Note how the current magnitude affects m_z switching.

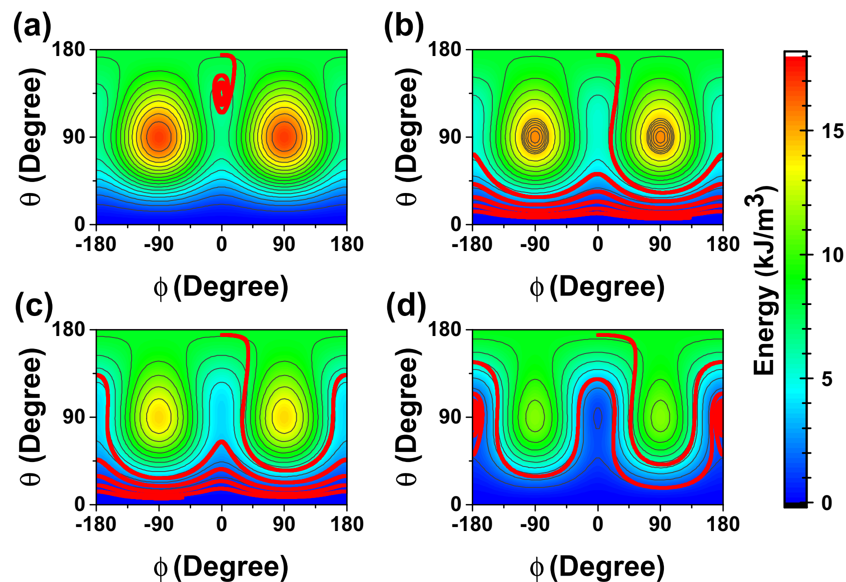

Figure 3. Magnetization trajectory (thick solid line) mapped on the energy contour plots at I_{wup} of (**a**) 3 μA, (**b**) 3.5 μA, (**c**) 4 μA, and (**d**) 5 μA. Higher current leads to the formation of energy minima at $\pm x$-direction.

formed near the x-axis, as can be seen in Fig. 3c. The magnetization dwells into these pockets, thus increasing the switching delay. Eventually, at the current of 5 μA, these "pockets" deepen, and the magnetization vector is trapped in them (see Fig. 3d). Thus, to prevent the formation of "pockets" an appropriate magnitude of current should be used. The study shows that current margin can be increased by decreasing the aspect ratio (AR). However, the switching delay will be degraded.

Analysis of performance sensitivity to material parameters

Delay versus current density and energy consumption versus current density plots for a baseline design are shown in Fig. 4a and b, respectively. The current was swept from a lower critical switching value of 54.54 kA/cm^2 to the maximum value of 90.91 kA/cm^2, since higher current densities lead to the loss of deterministic switching. As can be seen, the switching delay does not monotonically increase with the current. An optimal point with 6.25 ns and 75.91 fJ was observed at 77.82 kA/cm^2. At higher currents, switching energy rises significantly, whereas delay decreases negligibly.

Next, the effect of the damping constant α was studied. Generally, a higher damping constant is preferred because it improves both delay and energy consumption. A high α can be achieved by decreasing FL thickness or choosing optimal annealing temperature during stack formation[41,42]. For $\alpha = 0.075$, optimal delay decreases to 4.87 ns with 52.51 fJ energy, whereas for $\alpha = 0.025$, they are 9.91 ns and 116.52 fJ, respectively.

VCMA coefficient ξ has a notable effect on the delay. For $\xi = 30$ fJ/V·m, delay changes in the range of 5.96–3.39 ns, whereas, for $\xi = 200$ fJ/V·m, its range is 12.09–8.48 ns. Such behavior can be explained by a steeper energy density landscape at high ξ. When the energy landscape is steep, magnetization gets less acceleration

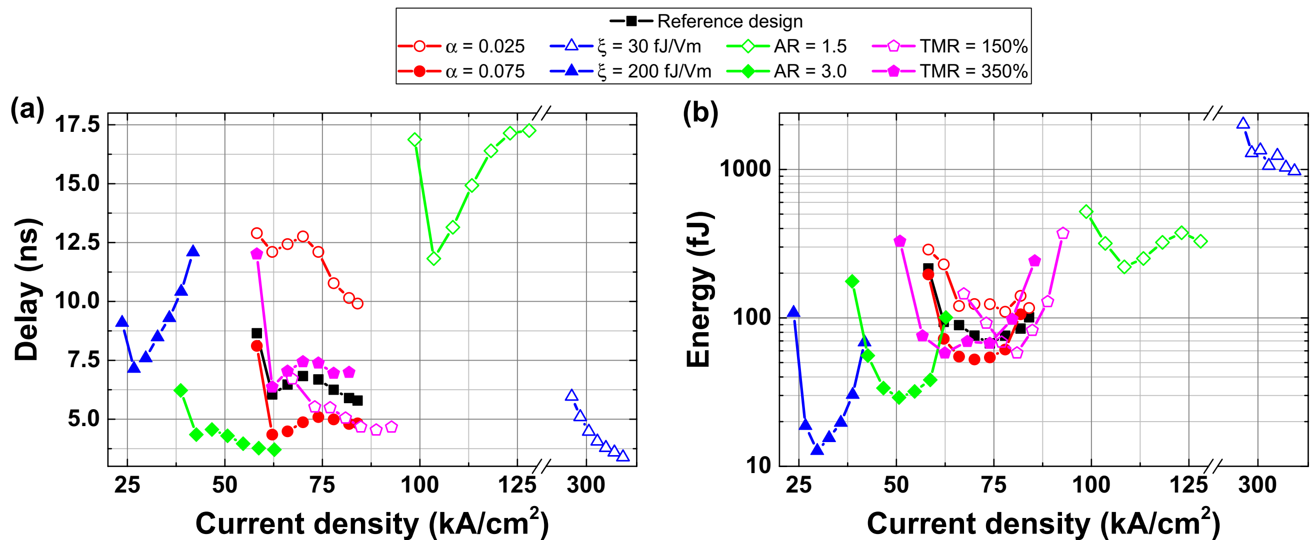

Figure 4. (**a**) Delay versus current density characteristics (in linear scale) and (**b**) energy versus current density characteristics (in logarithmic scale) sensitivity to changing material parameters with respect to the baseline design. Baseline design has $\alpha = 0.05$, $\xi = 100$ fJ/V·m, AR = 2.2, TMR = 250% is shown as rectangles.

from the effective in-plane demagnetizing field; therefore, the switching delay is higher. The major effect of ξ is the change in operating current margin, which leads to a decrease in energy. The current is on the order of hundreds of kA/cm^2 for 30 fJ/V·m and tens of kA/cm^2 for 200 fJ/V·m. It resulted in a drastic change of energy from 975.24 to 12.71 fJ. Note that $\xi > 200$ fJ/V·m is theoretically predicted for FePt/MgO interface[20,21], and $\xi > 300$ fJ/V·m was experimentally demonstrated for Fe/MgO[38].

The effect of changing the AR was studied by fixing the width to $W = 50$ nm while changing the length of the MTJ. As can be seen in Fig. 4a and b, AR = 1.5 results in considerable performance degradation: delay is on the order of 10 ns, and energy is ~200 fJ. AR = 3 improves both delay and energy consumption compared to the baseline design. They are as low as 3.77 ns and 38.22 fJ, respectively. It can be concluded that even though shape anisotropy is not necessary for the switching, its effect can be significant. However, the maximum AR of the MTJ may also be limited by manufacturing reasons.

Decreasing the TMR ratio leads to a minor delay improvement. It also can be explained by decreased energy slope for lower TMR. At TMR = 150% optimal point is 5.05 ns with 58.04 fJ, which is achieved at 80.91 kA/cm^2. If TMR is increased to 350%, the optimum becomes 7.04 ns with 57.90 fJ at 62.36 kA/cm^2. Note that energy consumption was reduced compared to the baseline design.

Although high α and ξ are desired for the DFFSP switching, they are process-defined. Consequently, their optimization involves considerable effort. In contrast, AR can be easily changed to improve cell performance. However, if the width of the MTJ equals minimal feature length F, AR can only be increased with the cell area.

DFFSP performance benchmarking

DFFSP was benchmarked to other switching methods frequently reported in the literature, such as STT, MFPV, FFPV, and PSTT. For a fair comparison, the material parameters from Table 1 were kept constant and only the stack geometry was optimized. Experimental results for VSOT[19,28] and DFFV[30] were included for the sake of comparison.

STT magnetization reversal is purely current-induced and favors low-resistivity junctions[5,6]. As can also be seen from Eq. (3), STT is inversely proportional to the FL thickness. Therefore, oxide and FL thicknesses were reduced to 1.1 nm. At such t_{ox}, $RA_p = 32.98\ \Omega \cdot \mu m^2$, TMR = 75%[39,40]. MTJ area was 50 × 50 nm^2. STT performance was evaluated at different current densities, below the barrier breakdown threshold.

For MFPV and FFPV, t_f was set to 1.1 nm, because $E_{VCMA} \propto 1/t_f$. For MFPV benchmarking, in-plane ExMF $H_x = 20$ kA/m was assumed to be generated from the current-carrying copper word line. Cell spacing of $2W = 100$ nm and wire cross-section of 160×10 nm^2 was considered. According to our simulations, a current of ≈ 7 mA is required to generate such a field. The power associated with one cell was 51.45 μW. In case of FFPV, $H_x = 4$ kA/m was assumed to originate from the antiferromagnet.

The PSTT method uses two sub-pulses: a high-voltage sub-pulse to utilize VCMA and a low-voltage sub-pulse to utilize STT. It requires the injection of non-negligible current during the second sub-pulse. Hence, $t_{ox} = 1.4$ nm with $RA_p = 186.11\ \Omega \cdot \mu m^2$ was used. Delay and energy consumption were evaluated for different voltage magnitudes of both sub-pulses. The duration of the first sub-pulse was chosen to avoid false switching. ExMF was excluded from the simulations to study the field-free performance of this method.

Figure 5 shows the results of benchmarking. STT switching is the most energy-demanding with a mean delay of 7.74 ns and mean writing energy of 1470 fJ. The MFPV has a delay of 0.68 ns, which is the fastest among the compared methods. However, the energy is 36.80 fJ. Note that energy dissipated on the MTJ (~1.8 fJ) is only a small share of the total energy. FFPV method with a 2.0 ns delay is a few times slower, compared

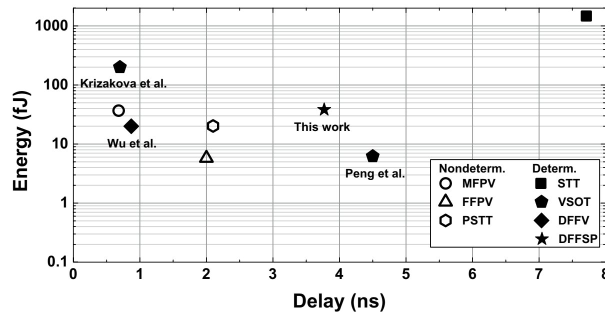

Figure 5. Comparison of switching delay and corresponding switching energy for different switching methods.

to its field-assisted counterpart, but its advantage is the low energy consumption of 6.22 fJ. The PSTT method has a delay of 2.10 ns and energy of 22.31 fJ. For VSOT method, two studies were considered. In the study of Peng et al.[19] delay of ~4.5 ns with 6.2 fJ energy was shown. Krizakova et al.[28] reported sub-nanosecond delay of 0.7 ns, but they did not mentioned switching energy. We approximately estimate energy losses on the order of 200 fJ, considering relatively large current densities. Wu et al. demonstrated DFFV MTJ switching with 0.87 ns delay and 20 fJ. The proposed DFFSP method is slower than traditional field-free methods with a delay of 3.77 ns and energy of 38.22 fJ. However, we emphasize that a pre-read-free, single-pulse operation may compensate for the difference in delay and energy. Note that a flat comparison in terms of the delay and energy may give an incomplete picture. A more detailed comparison of the switching methods is given in Table 2.

Discussion

In summary, we proposed a DFFSP magnet switching method. Unlike the other switching methods, DFFSP utilizes angle dependence of MTJ resistance in order to create energy asymmetry under a constant current. This energy asymmetry favors the parallel state. Therefore, deterministic switching was achieved by the implementation of a double-barrier MTJ structure, which has a benificial interface anisotropy constant and large TMR. DFFSP method demonstrates mean switching delay of 3.77 ns with energy consumption of 38.22 fJ. Furthermore, it combines robust deterministic writing, control simplicity, and energy efficiency to be used in low-power memory applications with low WER.

Even though DFFSP does not have a lower delay compared to other VCMA switching methods, it does not require a pre-read operation nor precise pulse timing, which would reduce WER significantly and dependence on error correction circuitry. Along with low operating current density, DFFSP switching double-barrier MTJ device is a viable candidate for deterministic, high precision, low-power memory applications.

Methods

The motion of the magnetization vector $\vec{m}$ was modeled by the Landau–Lifshitz–Gilbert (LLG) equation:

$$\frac{d\vec{m}}{dt} = -\frac{\gamma_0}{(1+\alpha^2)}\left[\vec{m}\times\vec{H}_{eff} - \frac{\alpha}{\gamma_0}\vec{m}\times\frac{d\vec{m}}{dt} - \frac{PI_s\hbar}{2q\mu_0 M_s V_f}\vec{m}\times(\vec{m}\times\vec{m}_p)\right] \quad (1)$$

where γ_0 is the gyromagnetic ratio; α is the damping constant; $\vec{H}_{eff}$ is the effective field; and the last term represents damping STT. Note that due to the low current, STT is significantly lower than the field torque, and its effect can be neglected. Here it was introduced for the sake of completeness. The remaining notations are as follows: P is the spin polarization; $\hbar$ is the reduced Planck's constant; q is the elementary charge; μ_0 is the vacuum

	STT	MFPV	FFPV	PSTT	VSOT	DFFV[30]	DFFSP (This work)
Delay (ns)	7.74	0.68	2.0	2.1	4.5[19], 0.7[28]	0.87	3.77
Energy (fJ)	1470	36.8	6.22	22.31	6.2[19], ~200[28]	20	38.22
Current density (MA/cm^2)	4.6	0.09 (MTJ) 437 (wire)	0.09	0.33	5[19], 170[28]	–	0.06
Pre-read	Not needed	Essential	Essential	Essential	Not needed	Not needed	Not needed
Pulse timing control	Not needed	Essential	Essential	Two pulses (consecutive)	Two pulses (simultaneous)	Two pulses (consecutive)	Not needed
ExMF (kA/m)	No	20	No*	No*	No*	No**	No
WER	$< 10^{-9}$	10^{-6}[14–16]	$4.5 \cdot 10^{-3}$	$< 10^{-4}$	–	$\sim 10^{-4}$	$< 10^{-9}$

Table 2. Performance benchmarking and requirements among switching methods. *Small bias field $H_x = 4$ kA/m provided from the antiferromagnetic stack to assist switching[17–19]. **Small stray field $H_z = 4$ kA/m provided from the permanent magnet[30].

permittivity; M_s is the saturation magnetization; V_f is the volume of free layer; $\vec{m}_p$ is the PL's magnetization. $\vec{H}_{eff}$ can be expressed in terms of the free energy density as[4,5,13,43]:

$$\vec{H}_{eff} = -\frac{1}{\mu_0 M_s}\frac{dE_{tot}}{d\vec{m}} + \vec{H}_{th} \tag{2}$$

$$E_{tot} = -\frac{K_i}{t_f}m_z^2 + \frac{\xi I_s R(\theta, V_b)}{t_f t_{ox}}m_z^2 + \frac{M_s^2\mu_0}{2} \times (N_x m_x^2 + N_y m_y^2 + N_z m_z^2) \tag{3}$$

where E_{tot} is the total free energy density, which consists of anisotropy, VCMA, and demagnetization energy terms. K_i is the interface anisotropy constant; t_f is the FL thickness; t_{ox} is the oxide thickness; ξ is the VCMA coefficient; N_x, N_y, N_z are the demagnetizing factors. Random field $\vec{H}_{th}$ models the Brownian motion of the magnetization and is given as follows:

$$\vec{H}_{th} = \vec{\sigma}\sqrt{2k_B T\alpha/(\gamma_0\mu_0 M_s V_f \Delta t)} \tag{4}$$

where k_B is the Boltzmann constant; T is the temperature; Δt time discretization step; and $\vec{\sigma}$ is the vector whose elements are the Gaussian distributed random numbers.

The thermal stability factor was calculated by the following analytical formula:

$$\Delta = \frac{E_b}{k_B T} = \frac{(K_i/t_f - 0.5M_s^2[N_z - N_y]) \cdot V_f}{k_B T} \tag{5}$$

Resistance is modeled as the following equation[4]:

$$R(\theta, V_b) = R_p\frac{1 + (V_b/V_h)^2 + TMR}{1 + (V_b/V_h)^2 + TMR[1/2 \cdot (1 + cos\theta)]} \tag{6}$$

where R_p is the resistance in parallel state and V_h is the voltage at which R_{ap} halves. The equation is solved self-consistently.

In this study, LLG was used within the single-domain approximation. Typically, such a model is used for describing small enough magnetic structures where the demagnetizing energy is insufficient to divide the material into multiple domains. It cannot account for a few second-order effects; however, it is still viable in illustrating physics-based device operation.

Spintronic devices are susceptible to thermal fluctuations; therefore, switching delay has stochastical distribution. To evaluate this distribution, Monte Carlo simulations with varying thermal field and initial angle θ_0 were performed. The number of attempts was $n_{at} = 10\,000$. Distribution of the θ_0 was obtained by device simulation at $V_b = 0$ V. We found that θ_0 varied from 152.07° to 180° with a mean value of 173.30°. The θ_0 was sampled over a 1 μs period with a sampling frequency of f_s = 4 THz. This distribution was used to generate the initial position for each attempt.

To study better ways of performance optimization, material sensitivity analysis was performed. Parameters listed in Table 1 were chosen as a baseline. Damping constant α, VCMA coefficient ξ, TMR, and AR were varied one by one while the remaining parameters were fixed. The only exception is the interface anisotropy K_i, which was changed to keep thermal stability factor Δ constant. Switching delay and energy distributions were obtained by Monte Carlo simulations considering the random thermal fluctuations. The switching threshold was set as $m_z = 0.9$.

Data availability

The data that support the findings of this study are available from the corresponding author upon reasonable request.

Received: 7 July 2023; Accepted: 22 September 2023
Published online: 26 September 2023

References

1. Maruyama, T. *et al.* Large voltage-induced magnetic anisotropy change in a few atomic layers of iron. *Nat. Nanotechnol.* **4**, 158–161. https://doi.org/10.1038/nnano.2008.406 (2009).
2. Meisenheimer, P. B., Novakov, S., Vu, N. M. & Heron, J. T. Perspective: Magnetoelectric switching in thin film multiferroic heterostructures. *J. Appl. Phys.* **123**, 240901. https://doi.org/10.1063/1.5031446 (2018).
3. Wang, K. L. *et al.* Electric-field control of spin-orbit interaction for low-power spintronics. *Proc. IEEE* **104**, 1974–2008. https://doi.org/10.1109/JPROC.2016.2573836 (2016).
4. Kang, W., Ran, Y., Zhang, Y., Lv, W. & Zhao, W. Modeling and exploration of the voltage-controlled magnetic anisotropy effect for the next-generation low-power and high-speed MRAM applications. *IEEE Trans. Nanotechnol.* **16**, 387–395. https://doi.org/10.1109/TNANO.2017.2660530 (2017).
5. Fong, X., Venkatesan, R., Raghunathan, A. & Roy, K. Non-volatile complementary polarizer spin-transfer torque on-chip caches: A device/circuit/systems perspective. *IEEE Trans. Magn.* **50**, 1–11. https://doi.org/10.1109/TMAG.2014.2326858 (2014).
6. Sin, S. & Oh, S. Lateral double magnetic tunnel junction device with orthogonal polarizer for high-performance magnetoresistive memory. *Sci. Rep.* **12**, 19762. https://doi.org/10.1038/s41598-022-24075-y (2022).
7. Shao, Q. *et al.* Roadmap of spin-orbit torques. *IEEE Trans. Magn.* **57**, 1–39. https://doi.org/10.1109/TMAG.2021.3078583 (2021).
8. Kanai, S., Matsukura, F. & Ohno, H. Electric-field-induced magnetization switching in CoFeB/MgO magnetic tunnel junctions with high junction resistance. *Appl. Phys. Lett.* **108**, 192406. https://doi.org/10.1063/1.4948763 (2016).

9. Shiota, Y. *et al.* Pulse voltage-induced dynamic magnetization switching in magnetic tunneling junctions with high resistance-area product. *Appl. Phys. Lett.* **101**, 102406. https://doi.org/10.1063/1.4751035 (2012).
10. Grezes, C. *et al.* Ultra-low switching energy and scaling in electric-field-controlled nanoscale magnetic tunnel junctions with high resistance-area product. *Appl. Phys. Lett.* **108**, 012403. https://doi.org/10.1063/1.4939446 (2016).
11. Shiota, Y. *et al.* Induction of coherent magnetization switching in a few atomic layers of FeCo using voltage pulses. *Nat. Mater.* **11**, 39–43. https://doi.org/10.1038/nmat3172 (2012).
12. Kang, W., Ran, Y., Lv, W., Zhang, Y. & Zhao, W. High-speed, low-power, magnetic non-volatile flip-flop with voltage-controlled, magnetic anisotropy assistance. *IEEE Magn. Lett.* **7**, 1–5. https://doi.org/10.1109/LMAG.2016.2604205 (2016).
13. Miriyala, V. P. K., Fong, X. & Liang, G. Influence of size and shape on the performance of VCMA-based MTJs. *IEEE Trans. Electron Devices* **66**, 944–949. https://doi.org/10.1109/TED.2018.2889112 (2019).
14. Song, J. *et al.* Evaluation of operating margin and switching probability of voltage- controlled magnetic anisotropy magnetic tunnel junctions. *IEEE J. Explor. Solid-State Comput. Devices Circuits* **4**, 76–84. https://doi.org/10.1109/JXCDC.2018.2880205 (2018).
15. Ikeura, T. *et al.* Reduction in the write error rate of voltage-induced dynamic magnetization switching using the reverse bias method. *Jpn. J. Appl. Phys.* **57**, 040311. https://doi.org/10.7567/jjap.57.040311 (2018).
16. Shiota, Y. *et al.* Evaluation of write error rate for voltage-driven dynamic magnetization switching in magnetic tunnel junctions with perpendicular magnetization. *Appl. Phys. Express* **9**, 013001. https://doi.org/10.7567/apex.9.013001 (2015).
17. Lau, Y.-C., Betto, D., Rode, K., Coey, J. M. D. & Stamenov, P. Spin-orbit torque switching without an external field using interlayer exchange coupling. *Nat. Nanotechnol.* **11**, 758–762. https://doi.org/10.1038/nnano.2016.84 (2016).
18. Oh, Y.-W. *et al.* Field-free switching of perpendicular magnetization through spin-orbit torque in antiferromagnet/ferromagnet/oxide structures. *Nat. Nanotechnol.* **11**, 878–884. https://doi.org/10.1038/nnano.2016.109 (2016).
19. Peng, S. Z. *et al.* Field-free switching of perpendicular magnetization through voltage-gated spin-orbit torque. In *2019 IEEE International Electron Devices Meeting (IEDM)*, 28.6.1–28.6.4. https://doi.org/10.1109/IEDM19573.2019.8993513.
20. Yi, M., Zhang, H. & Xu, B.-X. Voltage-driven charge-mediated fast 180 degree magnetization switching in nanoheterostructure at room temperature. *npj Comput. Mater.* **3**, 38. https://doi.org/10.1038/s41524-017-0043-x (2017).
21. Gong, Q., Yi, M. & Xu, B.-X. Electric field induced magnetization reversal in magnet/insulator nanoheterostructure. *Int. J. Smart Nano Mater.* **11**, 298–309. https://doi.org/10.1080/19475411.2020.1815132 (2020).
22. Lee, H. *et al.* Design of a fast and low-power sense amplifier and writing circuit for high-speed MRAM. *IEEE Trans. Magn.* **51**, 1–7. https://doi.org/10.1109/TMAG.2014.2367130 (2015).
23. Wang, S. *et al. MTJ variation monitor-assisted adaptive MRAM write*. https://doi.org/10.1145/2897937.2897979 (2016).
24. Long, M. *et al.* Self-adaptive write circuit for magnetic tunneling junction memory with voltage-controlled magnetic anisotropy effect. *IEEE Trans. Nanotechnol.* **17**, 492–499. https://doi.org/10.1109/TNANO.2018.2815721 (2018).
25. Wang, S. *et al.* Adaptive MRAM write and read with MTJ variation monitor. *IEEE Trans. Emerg. Top. Comput.* **9**, 402–413. https://doi.org/10.1109/TETC.2018.2866289 (2021).
26. Kanai, S. *et al.* Magnetization switching in a CoFeB/MgO magnetic tunnel junction by combining spin-transfer torque and electric field-effect. *Appl. Phys. Lett.* **104**, 212406. https://doi.org/10.1063/1.4880720 (2014).
27. Luo, Z. Y., Tsou, Y. J., Dong, Y. C., Lu, C. & Liu, C. W. Field-free spin-orbit torque switching of perpendicular magnetic tunnel junction utilizing voltage-controlled magnetic anisotropy pulse width optimization. In *2018 Non-Volatile Memory Technology Symposium (NVMTS)*, 1–5. https://doi.org/10.1109/NVMTS.2018.8603107.
28. Krizakova, V., Garello, K., Grimaldi, E., Kar, G. S. & Gambardella, P. Field-free switching of magnetic tunnel junctions driven by spin-orbit torques at sub-ns timescales. *Appl. Phys. Lett.* **116**, 232406. https://doi.org/10.1063/5.0011433 (2020).
29. Zhang, K. *et al.* Compact modeling and analysis of voltage-gated spin-orbit torque magnetic tunnel junction. *IEEE Access* **8**, 50792–50800. https://doi.org/10.1109/ACCESS.2020.2980073 (2020).
30. Wu, Y. C. *et al.* Deterministic and field-free voltage-controlled mram for high performance and low power applications. In *2020 IEEE Symposium on VLSI Technology*, 1–2. https://doi.org/10.1109/VLSITechnology18217.2020.9265057.
31. Lee, S.-E., Takemura, Y. & Park, J.-G. Effect of double MgO tunneling barrier on thermal stability and TMR ratio for perpendicular MTJ spin-valve with tungsten layers. *Appl. Phys. Lett.* **109**, 182405. https://doi.org/10.1063/1.4967172 (2016).
32. Sato, H. *et al.* Perpendicular-anisotropy CoFeB-MgO magnetic tunnel junctions with a MgO/CoFeB/Ta/CoFeB/MgO recording structure. *Appl. Phys. Lett.* **101**, 022414. https://doi.org/10.1063/1.4736727 (2012).
33. Sato, H. *et al.* Properties of magnetic tunnel junctions with a MgO/CoFeB/Ta/CoFeB/MgO recording structure down to junction diameter of 11 nm. *Appl. Phys. Lett.* **105**, 062403. https://doi.org/10.1063/1.4892924 (2014).
34. Lee, D.-Y., Hong, S.-H., Lee, S.-E. & Park, J.-G. Dependency of tunneling-magnetoresistance ratio on nanoscale spacer thickness and material for double MgO based perpendicular-magnetic-tunneling-junction. *Sci. Rep.* **6**, 38125. https://doi.org/10.1038/srep38125 (2016).
35. Iwata-Harms, J. M. *et al.* High-temperature thermal stability driven by magnetization dilution in CoFeB free layers for spin-transfer-torque magnetic random access memory. *Sci. Rep.* **8**, 14409. https://doi.org/10.1038/s41598-018-32641-6 (2018).
36. Couet, S. *et al.* Impact of Ta and W-based spacers in double MgO STT-MRAM free layers on perpendicular anisotropy and damping. *Appl. Phys. Lett.* **111**, 152406. https://doi.org/10.1063/1.5000992 (2017).
37. Li, X. *et al.* Enhancement of voltage-controlled magnetic anisotropy through precise control of Mg insertion thickness at CoFeB MgO interface. *Appl. Phys. Lett.* **110**, 052401. https://doi.org/10.1063/1.4975160 (2017).
38. Nozaki, T. *et al.* Highly efficient voltage control of spin and enhanced interfacial perpendicular magnetic anisotropy in iridium-doped Fe/MgO magnetic tunnel junctions. *NPG Asia Mater.* **9**, e451–e451. https://doi.org/10.1038/am.2017.204 (2017).
39. Isogami, S. *et al.* In situ heat treatment of ultrathin MgO layer for giant magnetoresistance ratio with low resistance area product in CoFeB/MgO/CoFeB magnetic tunnel junctions. *Appl. Phys. Lett.* **93**, 192109. https://doi.org/10.1063/1.3021372 (2008).
40. Hayakawa, J., Ikeda, S., Matsukura, F., Takahashi, H. & Ohno, H. Dependence of giant tunnel magnetoresistance of sputtered CoFeB/MgO/CoFeB magnetic tunnel junctions on MgO barrier thickness and annealing temperature. *Jpn. J. Appl. Phys.* **44**, L587–L589. https://doi.org/10.1143/jjap.44.l587 (2005).
41. Cui, Y. *et al.* Interfacial perpendicular magnetic anisotropy and damping parameter in ultra thin Co_2FeAl films. *Appl. Phys. Lett.* **102**, 162403. https://doi.org/10.1063/1.4802952 (2013).
42. Iihama, S. *et al.* Gilbert damping constants of Ta/CoFeB/MgO(Ta) thin films measured by optical detection of precessional magnetization dynamics. *Phys. Rev. B* **89**, 174416. https://doi.org/10.1103/PhysRevB.89.174416 (2014).
43. Xiao, J., Zangwill, A. & Stiles, M. D. Macrospin models of spin transfer dynamics. *Phys. Rev. B* **72**, 014446. https://doi.org/10.1103/PhysRevB.72.014446 (2005).

Acknowledgements

This work was supported in part by the National Research Foundation of Korea (NRF) funded by the Ministry of Science and ICT (MSIT) of the Korea Government under grants 2021R1F1A1060444, 2022M3F3A2A01073562, and 2022M3F3A2A01072215.

Author contributions

S.S. proposed the idea for the work and performed simulations. S.S. and S.O. analyzed the data and wrote the manuscript. Both authors have given approval to the final version of the manuscript.

Competing interests

The authors declare no competing interests.

Additional information

Correspondence and requests for materials should be addressed to S.O.

Reprints and permissions information is available at www.nature.com/reprints.

Publisher's note Springer Nature remains neutral with regard to jurisdictional claims in published maps and institutional affiliations.

Open Access This article is licensed under a Creative Commons Attribution 4.0 International License, which permits use, sharing, adaptation, distribution and reproduction in any medium or format, as long as you give appropriate credit to the original author(s) and the source, provide a link to the Creative Commons licence, and indicate if changes were made. The images or other third party material in this article are included in the article's Creative Commons licence, unless indicated otherwise in a credit line to the material. If material is not included in the article's Creative Commons licence and your intended use is not permitted by statutory regulation or exceeds the permitted use, you will need to obtain permission directly from the copyright holder. To view a copy of this licence, visit http://creativecommons.org/licenses/by/4.0/.

© The Author(s) 2023